Journal of Non-Crystalline Solids 113 (1989) 41–50
North-Holland, Amsterdam

STRUCTURAL STUDIES OF AMORPHOUS Si : Ni : H

A.M. EDWARDS, M.C. FAIRBANKS, R.J. NEWPORT, S.J. GURMAN [a] and E.A. DAVIS [a]

Physics Laboratory, University of Kent, Canterbury, Kent, CT2 7NR, UK
[a] *Physics Department, University of Leicester, Leicester, LE1 7RH, UK*

Received 11 April 1989

It is well known that the transition from an insulator to a metallic conductor may be induced in amorphous semiconductor : metal alloys by increasing the metal concentration above a certain critical limit. However, without a detailed understanding of the changes taking place in the atomic scale structure, it is difficult to ascribe a mechanism to the process. We have investigated the microstructure of one such alloy system, a-$Si_{1-y}Ni_yH$, using EXAFS as the principal technique. Thin film samples, prepared by rf co-sputtering, were studied over the composition range $0 < y < 0.3$. Both silicon and nickel K-edge EXAFS results are presented, together with complementary data from Raman scattering, neutron diffraction and scanning calorimetry experiments. The results indicate that the samples contain two separate amorphous phases: a Ni : Si alloy which is embedded in the surviving, modified a-Si host network. The measured electrical conductivity is discussed in the light of this structural model.

1. Introduction

The existence of a metal–insulator transition (MIT) in a variety of systems has attracted considerable attention over the past decade for both fundamental and technological reasons. One such system involves the alloying of a-Si with d-band metals. By varying the composition, it is possible to control the electrical conductivity of the alloy. The conductivity increases with an increasing proportion of metal atoms until the latter rises above some critical limit which results in a transition from semiconducting to metallic behaviour. The alloying is thought to produce impurity levels deep within the intrinsic bandgap, and hence induce the MIT at a metal concentration of around 15% [1].

Early work on microcrystalline Si : Ni alloys [2] reported that the MIT occurred at 13 at% Ni, and this transition was assumed to be of Anderson type. This process involves the impurity states at the Fermi level becoming delocalised as the density of states rises. More recent work [3] on amorphous Si : Ni systems shows an enhancement of the DC conductivity by up to 8 orders of magnitude over that of amorphous silicon for as little as 5 at% Ni, but an optical gap remains up to about 25% Ni.

While much work has focussed on the MIT in such systems, few structural studies have been undertaken – yet it is far from obvious how the metal impurity atoms are incorporated into the amorphous semiconducting host. Without a more detailed knowledge of the atomic scale structure, the mechanisms responsible for the MIT cannot be fully understood. Therefore, we have investigated the structure of a-$Si_{1-y}Ni_yH$ over the composition range $0 < y < 0.3$.

2. Sample preparation and characterization

Thin films of a-$Si_{1-y}Ni_yH$ were prepared by rf reactive co-sputtering [4] under controlled conditions: an rf power of 200 W and a total gas pressure of 7.3 μbar. Argon of 99.998% purity was used as the sputtering gas, with 99.993% pure H_2 added in the ratio 10 : 1, Ar : H_2, to saturate dan-

0022-3093/89/$03.50 © Elsevier Science Publishers B.V.
(North-Holland Physics Publishing Division)

gling bonds in the films [5]. The metal content of the samples was altered by varying the number of Ni or $NiSi_2$ discs placed on the 10 cm diameter, crystalline Si target. These discs were arranged uniformly to give a homogeneous distribution at the substrate; the target–substrate separation was 5.5 cm. Substrates suitable for EXAFS, Raman spectroscopy, DC conductivity, IR absorption and electron microprobe analysis were held at ambient temperature during sample deposition.

Determination of the sample's thickness was undertaken using a profilometer (Talysurf). The sample composition was measured using the technique of energy dispersive electron microprobe analysis (and later checked by $^4He^+$ Rutherford backscattering), and was found to be uniform ($\pm y = 0.02$) for any particular Film. In addition to Si and Ni, immediately after deposition each sample was found to contain approximately 8 at% Ar, incorporated during the sputtering process. It is not possible to estimate the hydrogen content of the films by these methods; however, IR absorption measurements indicate, as expected, the presence of Si–H covalent bonds at all compositions. In addition, the IR spectra show no significant contamination of the samples by O_2 or N_2.

Optical reflectivity measurements in the UV and visible ranges, performed in a parallel study [6], show a large increase in absorption with the addition of even small amounts of Ni, the a-Si : H bandgap being reduced to very small values. This is supported by DC conductivity measurements [7] where a dramatic increase in conductivity, compared to that of the undoped a-Si : H, is obtained on the addition of a few percent Ni. These conductivity results show qualitative agreement with those made by Rogachev et al. [3], any quantitative differences probably being due to differing methods in the determination of sample composition.

Raman scattering provides an extremely sensitive test for the presence of c-Si, which produces a characteristic phonon peak at 522 cm^{-1}. In a-Si, this peak is broadened and shifted to around 480 cm^{-1}. The Raman spectra obtained using the 5145 Å line of an argon ion laser showed no evidence of c-Si in any of the samples, though the broader a-Si peak was present in all compositions.

3. EXAFS experiments

Extended X-ray absorption fine structure (EXAFS) data from both the silicon and the nickel K-edges were collected for samples in the composition range $0 < y < 0.3$ using the 2 GeV Synchrotron Radiation Source at the Daresbury Laboratory with beam currents between 150 and 250 mA.

Silicon K-edge experiments were performed on beamline 3.4 using a Cr-plated mirror to focus the beam at the sample. The energy of the X-ray beam was defined using an InSb double-crystal monochromator with a harmonic rejection set at 70%. The incident beam was monitored using an Al foil.

Absorption by the sample was measured using the electron drain current method, a modification of the total electron yield method [9] necessitating a conducting substrate. Samples of 1–2 μm thick films deposited on stainless steel substrates were used, the angle between the incident beam and the sample being varied to optimize the counting statistics.

Measurements on the nickel K-edge were performed on beamline 7.1 using a Si(111) double-crystal monochromator and a harmonic rejection of 50%. All these experiments were performed in transmission mode with detection by Ar/He gas ionization chambers [10]. In this case, 1–2 μm thick films were deposited on mylar substrates and stacked to obtain the optimum absorption–thickness product ($\mu t \sim 1–2$) at the absorption edge. More comprehensive beamline specifications for both 3.4 and 7.1 can be found elsewhere [8].

4. Data analysis

The transmission data was energy-calibrated by the EXCALIB program [11] available at the Daresbury Laboratory; while the EXBACKV program [11] was used to fit low-order polynomials to the smooth atomic absorption backgrounds (μ_0) of the pre- and post-edge data so that this could be subtracted from the spectra, leaving only the

EXAFS function, $X(k)$:

$$X(k) = \frac{\mu(k) - \mu_0(k)}{\mu_0(k)}. \quad (1)$$

To ensure that the pre-edge background subtraction was not affecting the data, three different pre-edge background subtractions were performed on a sample of c-Si. Comparison of the resulting Fourier transformations showed that, within experimental error, these variations in the pre-edge background subtraction did not significantly alter the data.

A simplified version of the EXAFS function for K-edges, which shows clearly the structural information contained in the spectra, is expressed by the equation [12]

$$X(k) = \sum_j \frac{-A(k)N_j}{(kR_j^2)} |F_j(\pi)| \exp(-2\sigma_j^2 k^2) \times \exp\left(\frac{-2R_J}{\lambda}\right) \sin(2kR_j + 2\delta + \Psi_j) \quad (2)$$

Here N_j is the number of neighbouring atoms in a shell of radius R_j around the absorbing atom, each having a backscattering amplitude $F_j(\pi)$ which is a function of both atom type and photoelectron momentum, k. $A(k)$ is an energy-independent factor which corrects for amplitude reductions due to events that result in absorption but not EXAFS (such as multiple excitations). The first exponential term is the Debye–Waller factor which provides a description of the static and thermal disorder of the system. σ_j^2 is the mean square deviation in interatomic distance, R_j. The second exponential term acts as a damping factor which accounts for losses by inelastic scattering and multielectron excitation, with λ being the elastic mean free path of the photoelectron. The phase shift experienced by the photoelectron on passage through the emitting atom potential is described by δ, while Ψ_j represents the phase of the backscattering factor.

Structural information was obtained by multiparameter fitting of the experimental data to the EXAFS function in k-space, using the least-squares routine available in the EXCURV88 curved wave package [13].

For the successful application of this method, it is necessary to use a reliable set of backscattering factors and phase shifts. For each atom type, a value of $F_j(\pi)$, calculated within EXCURV88, was used. The combined phase-shift $(2\delta + \Psi_j)$ was also calculated by the program and then empirically modified so that the structural parameters for the standard compounds, c-Si and Ni metal, agreed to within experimental error with their accepted values.

Transferability of the modified phase shifts to other systems was tested by using them to fit to data collected on three more known compounds – $NiSi_2$, SiO_2 and NiO. In each case, the element of interest is in a very different chemical environment to that of the original standards, yet the new phase shifts yielded reliable interactomic distances.

The amplitude factor (AFAC), which corrects for events such as multiple excitations, was varied on the standard samples to obtain a most likely value for each atom type, its magnitude was fixed at this "best" result thereafter. The photoelectron mean free path, λ, described in terms of an imaginary part of the potential (VPI) in the experimental fits, was allowed to float around the value obtained from the standard samples. The EXCURV88 fitting routine uses a non-linear least-squares fit for the fast curved wave theory [14] to the data, with interatomic distance (R), coordination number (N), Debye–Waller factor ($A = 2\sigma^2$) and energy offset (EO) as variable parameters. The edge was assumed to occur at the energy of the principal maximum in the first derivative of the near-edge raw data, and zero wavevector ($k = 0$) was taken as a value EO below this edge. The useful energy range of the spectra extended to 500–600 eV above the edge and Gaussian windows were used in the Fourier transformations. The quality of the fit of $X(k)$ to the experimental spectra may be quantified by using a parameter known as the fit index (FI), which is defined as

$$\mathrm{FI} = \frac{1}{100N_{\mathrm{pt}}} \sum_{i=1}^{N_{\mathrm{pt}}} \left[(X_i\ \mathrm{calc} - X_i\ \mathrm{expt})K^{\mathrm{wt}}\right]^2 \quad (3)$$

where N_{pt} = number of data points, and wt = integral k weighting factor.

A non-trivial problem encountered when using this type of curvefitting approach in the analysis of EXAFS data is the question of how many atomic shells to include. The addition of an extra shell may decrease the fit index slightly, but also increases the number of adjustable parameters in the fit. Thus, it is necessary to apply a rigorous statistical approach. We have used the criterion of Joyner et al. [15] to assess the significance of the addition of another shell. Each new shell (n) introduces 3 additional parameters (N_n, R_n and A_n), and for a typical set of around 200 data points the fit index needs to decrease by

$$\frac{FI_{n+1}}{FI_n} < 0.96, \quad (4)$$

to obtain a 5% level of significance (i.e. for the new shell to have a 95% probability of being meaningful). It is also useful to apply this approach to the evaluation of errors on individual parameters, and important to note that strong correlations often exist between parameters.

5. EXAFS results

5.1. Ni K-edge EXAFS results

Using the criterion above, we found that we were justified in fitting a 2-shell model to the Ni K-edge data, the results of which are shown in table 1 for the range $0.03 < y < 0.29$. Over this range, the EXAFS signal is remarkably constant in phase and amplitude (figs. 1 and 2) indicating that there is no observable change in the local environment of the Ni atoms. Each metal atom has approximately 8 nearest neighbours of Si at 2.35 Å and 3 Ni near-neighbours at 2.53 Å, resulting in a total coordination of around 11. This figure is surprisingly high given the assumption of a homogeneous alloy and suggests that some kind of clustering must occur around the Ni sites. However, this clustering cannot consist simply of metal atoms, but must also contain a sizeable proportion of Si atoms. This suggests that the Ni atoms do not enter the a-Si random network either substitutionally or interstitially, but rather form a closely packed Ni–Si alloy. The magnitude of EO in the fits was found to vary in the range 7.5–10.5 eV, while the value of VPI remained within 0.03 eV of the standard sample value of −5.5 eV.

5.2. Si K-edge EXAFS results

The structural parameters derived for the Si K-edge are summarized in table 2. For these results it was only meaningful to fit one shell to the data. These fits and their corresponding Fourier transforms are shown in figs. 3 and 4. EO was found to vary between 1.25 and 4.96 eV, while VPI ranged from −1 to −2.85 eV using a standard sample value of −2.0 eV. At low Ni content the Si K-edge EXAFS is dominanted by a-Si, but as the metallic content is increased we see a trend

Table 1
Nickel K-edge EXAFS results. AFAC = 0.75

y (at%)	N_{Ni-Si} (±1.0)	N_{Ni-Ni} (±1.0)	R_{Ni-Si} (±0.02 Å)	R_{Ni-Ni} (±0.02 Å)	A_{Ni-Si} (±0.003)	A_{Ni-Ni} (±0.005)
3.0	7.4	1.5	2.33	2.55	0.019	0.021
5.5	7.5	2.3	2.33	2.54	0.020	0.024
9.0	9.0	4.9	2.37	2.51	0.022	0.039
13.0	9.3	3.5	2.36	2.52	0.024	0.033
14.0	9.1	4.0	2.36	2.52	0.024	0.035
16.0	8.8	3.3	2.35	2.53	0.023	0.031
19.0	8.6	2.8	2.34	2.54	0.024	0.026
22.0	8.7	2.6	2.35	2.54	0.024	0.025
25.0	8.5	2.7	2.35	2.54	0.023	0.026
26.0	8.4	2.5	2.35	2.54	0.022	0.025
29.0	8.3	2.3	2.34	2.55	0.022	0.022

towards lower Si–Si coordination numbers and larger Si–Si distances due to the increasing contributions of the Ni–Si regions to the EXAFS signal. The gradual decrease in Si–Si coordination number with increasing nickel can be explained by the fact that the nickel and silicon backscattering phases differ by a factor close to π in the energy region of the experiment [16]. Therefore the nickel backscattering will tend to cancel that of the sili-

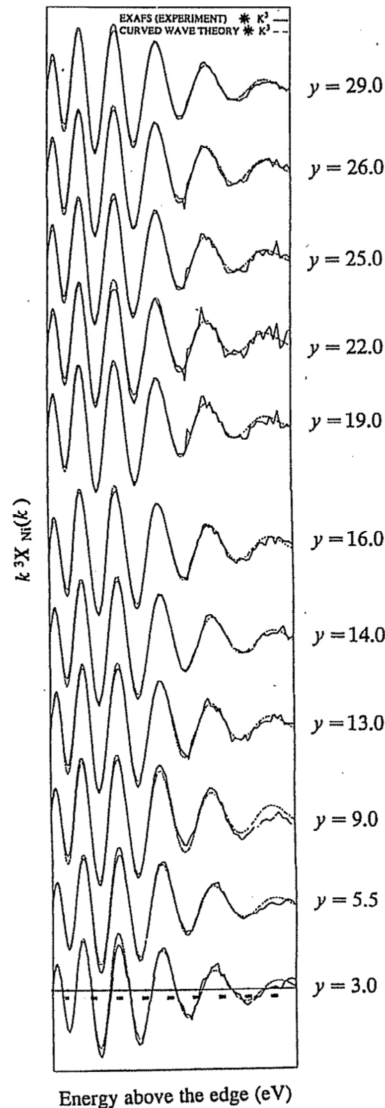

Fig. 1. Nickel K-edge EXAFS spectra. Fits of the Ni $k^3X(k)$ over the composition range $0.3 < y < 0.29$.

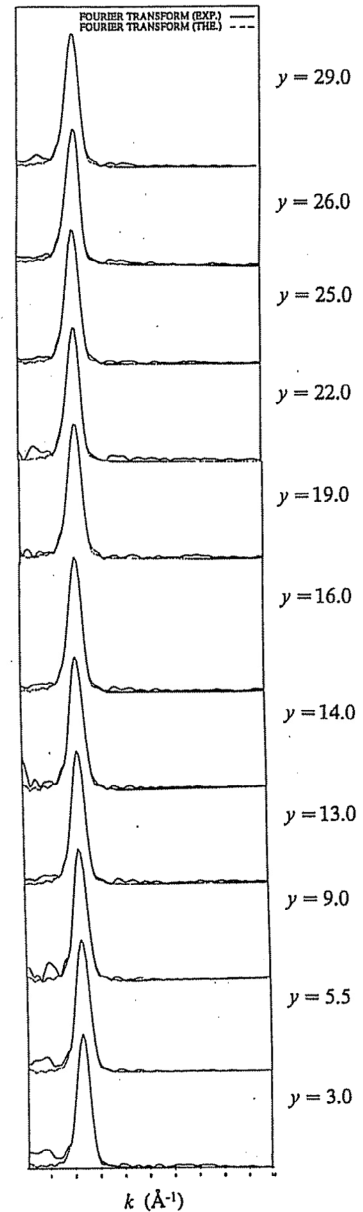

Fig. 2. Nickel K-edge Fourier transforms. Fourier transforms of the Ni $k^3X(k)$ over the composition range $0.3 < y < 0.29$.

con, causing the EXAFS to determine a Si–Si coordination number lower than the true one. Using the Ni–Si coordination given by the nickel edge data we can calculate the expected Si–Ni coordination, which shows an opposite trend to the Si–Si coordination and rises with increasing

Table 2
Silicon K-edge EXAFS results. AFAC = 0.70

y (at%)	N_{Si-Si} (± 0.8)	R_{Si-Si} (± 0.02 Å)	A_{Si-Si} (± 0.003)
0.0	4.0	2.35	0.007
3.0	3.0	2.35	0.003
5.5	2.6	2.36	0.002
9.0	2.7	2.34	0.003
13.0	2.8	2.34	0.005
16.0	2.2	2.35	0.005
19.0	2.4	2.35	0.005
22.0	1.8	2.36	0.006
25.0	1.1	2.39	0.009

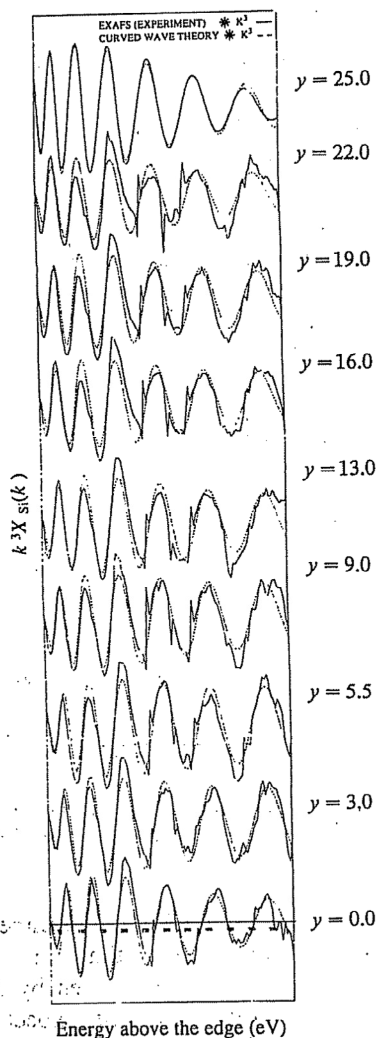

Fig. 3. Silicon K-edge EXAFS spectra. Fits of the Si $k^3X(k)$ over the composition range $0.0 < y < 0.25$.

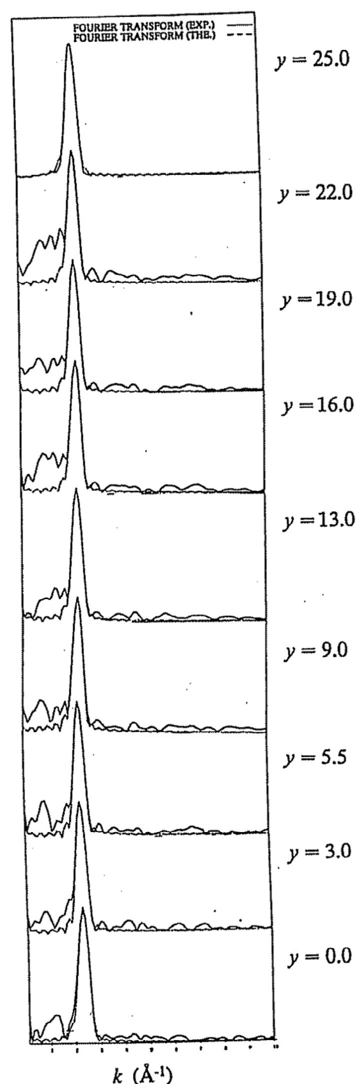

Fig. 4. Silicon K-edge Fourier transforms. Fourier transforms of the Si $k^3X(k)$ over the composition range $0.0 < y < 0.25$.

metal content, giving an average silicon coordination of 4. Resolution between Si–Si and Si–Ni distances (which we find to be of almost equal magnitude) is extremely difficult for the Si edge data, so that although the nickel must be contributing to the signal at higher values of y, only a near-neighbour shell of Si could be reliably fitted. However, not including a Ni shell introduces a phase problem at higher energies, since Si scatters at low energy only while the Ni scatters at higher

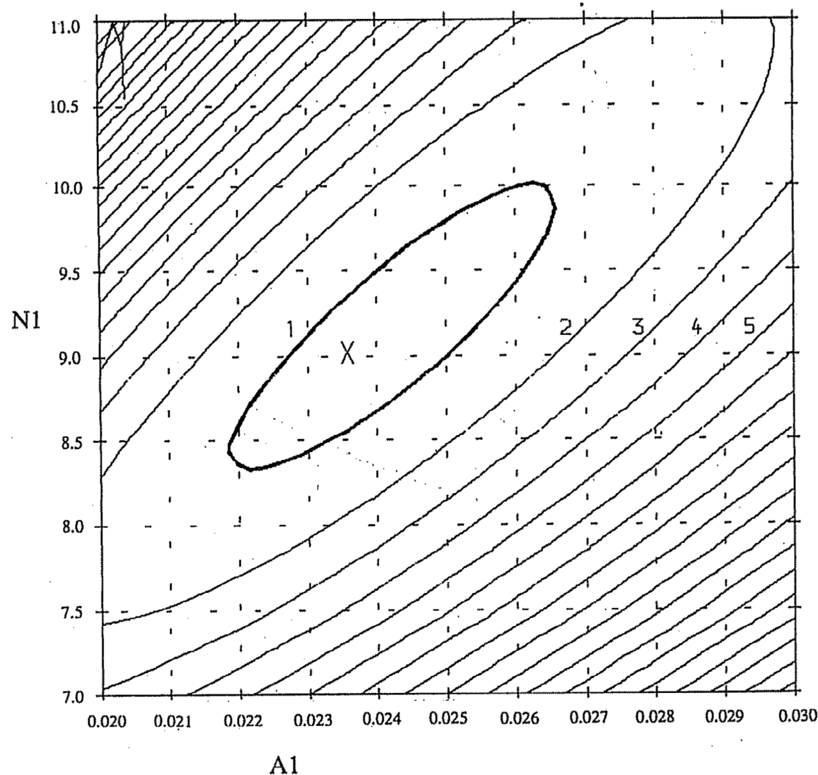

Fig. 5. Contour map for Ni K-edge first shell ($y = 0.13$) showing the correlation between $A1$ and $N1$.

energies. The increasing metal concentration also increases the overall absorption of the soft X-ray beam, decreasing the statistical accuracy of the spectra and producing an overall increase in the uncertainty of the results. Error estimates were taken from contour maps * such as those shown in figs. 5 and 6.

6. Discussion

EXAFS results from the Ni K-edge clearly indicate clustering of both Si and Ni atoms around the Ni sites in some form of Ni–Si alloy. The measured near-neighbour distances also correspond to those found in several of the crystalline Ni_xSi compounds [17]; however, a neutron scattering experiment performed on a single sample of a-$Si_{0.9}Ni_{0.1}D$ showed no evidence of crystallinity and hence we conclude that the clusters are not microcrystals of nickel silicide, but a disordered form of this alloy. Amorphous phases of Ni : Si are, in fact, observed at Ni–Si interfaces after the deposition of thin layers of metallic nickel onto crystalline silicon [18].

Raman spectroscopy indicates the presence of an a-Si matrix at all compositions with no evidence of c-Si (the narrow spikes at 5145 Å in fig. 7 being plasma lines from the Ar ion laser); taken with the previous conclusion, this suggests that the system contains two distinct amorphous regions, both containing Si. This further complicates interpretation of the Si K-edge results, since the EXAFS technique only returns coordination numbers and interatomic distances for the environment

* In EXCURV88, the limit of significance can be shown as a broad line on contour maps of the fit index over a range of parameter values. This is extremely helpful in indicating the degrees of any correlation and estimating the real errors involved, and it is these error estimates that are quoted in tables 1 and 2.

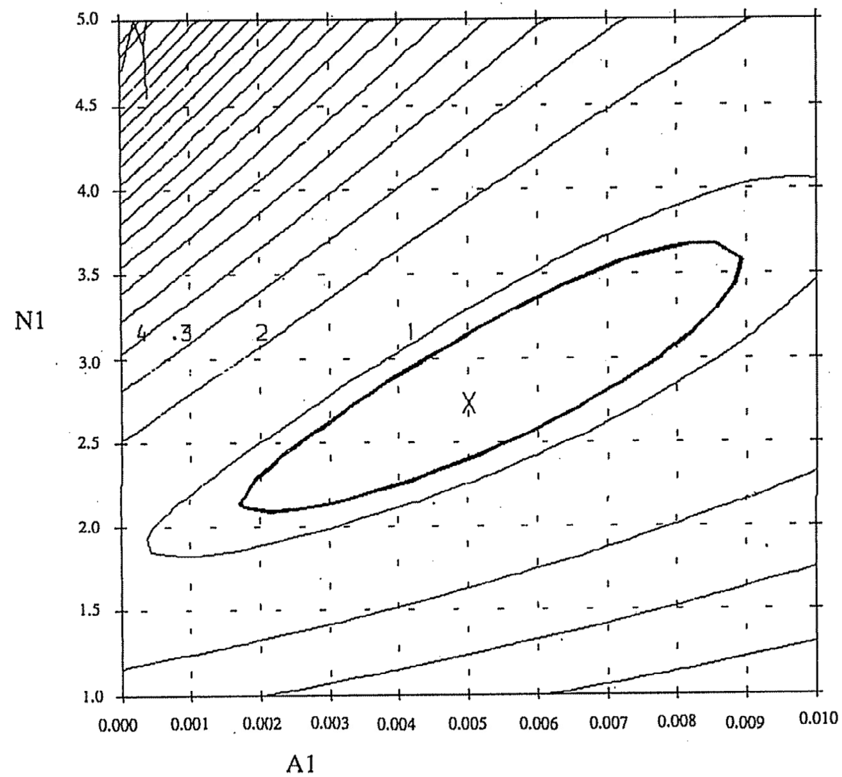

Fig. 6. Contour map for Si K-edge first shell ($y = 0.13$) showing the correlation between $A1$ and $N1$.

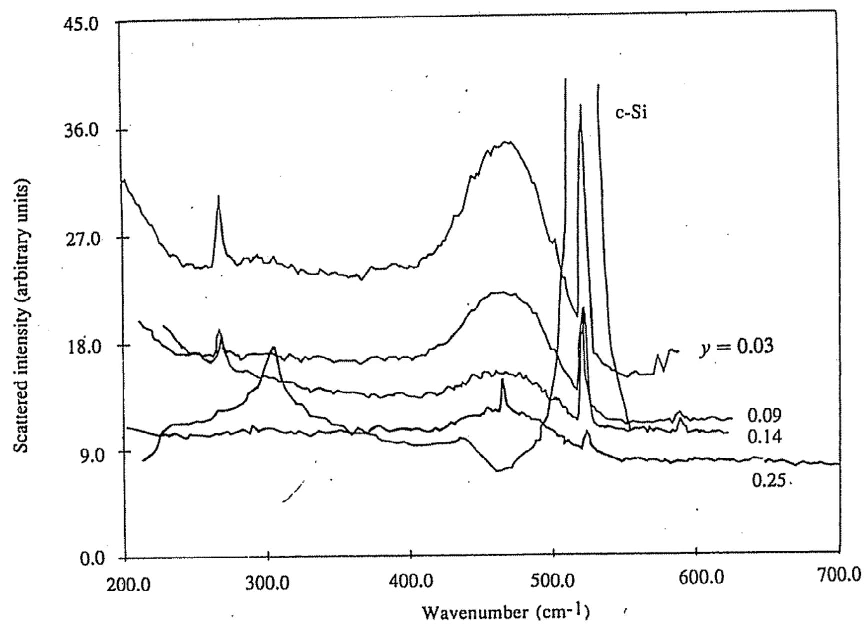

Fig. 7. Raman spectra of a-$Si_{1-y}Ni_y$: H compared to that of c-Si.

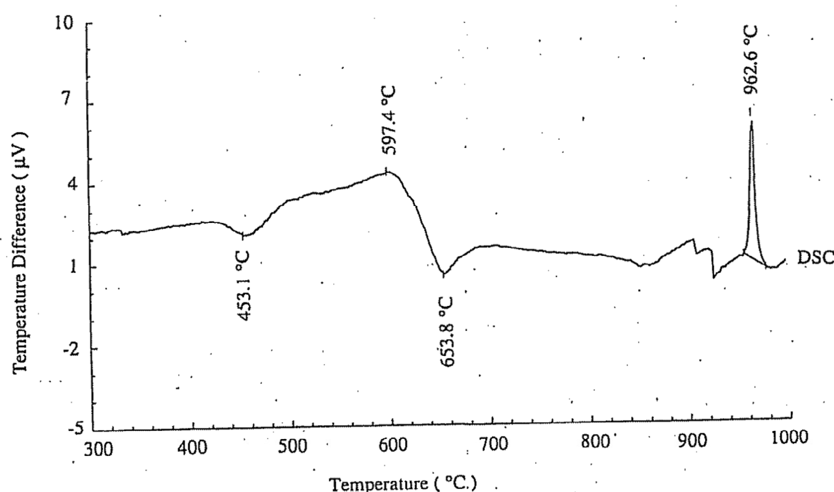

Fig. 8. Differential scanning calorimetry scan of a single sample of a-$Si_{0.9}Ni_{0.1}$: H.

around a specific atom averaged over all of the sites occupied by that atom. However, trends in the results suggest that the average Si–Si distance in the clusters is greater than that in a-Si and that the clusters contain more silicon than nickel. It is not clear whether it is the size or number of clusters that increases with increasing nickel, though the nickel EXAFS results show their composition to be roughly constant. Evidence for a two-phase system is further supported by the two recrystallization temperatures (450 and 650 ° C respectively) measured by differential scanning calorimetry on a single composition, $y = 0.1$ (fig. 8). X-ray diffraction on a laboratory source indicates that the former transition is associated with the formation of crystalline $NiSi_2$ having a fluorite structure. This compound is known to form readily at the interfaces of Ni–Si films on annealing. Although the minimum formation temperature of $NiSi_2$ for thick (> 200 Å) layers of Ni on c-Si is ~ 775 ° C, after the deposition of thin layers of the metal, $NiSi_2$ was found to form at the interface at 450 ° C [19]. The recrystallization temperature of 650 ° C is known to correspond to the crystallization of a-Si : H [5].

DC conductivity work [3] shows an enormous increase in conductivity for even small amounts of nickel, suggesting the possibility that the system exhibits metallic conduction well below the level of 15 at% metal concentration. If we now consider the material as a two-phase system consisting of an a-Si semiconducting matrix containing clusters of an amorphous Ni : Si alloy of higher conductivity, then some of the silicon in the sample will be contributing to those regions of greater conductivity. Therefore, a greater volume fraction of the sample will have an enhanced conductivity than would be estimated from a naive use of Ni content, and any transition is likely to occur at a lower Ni concentration than would otherwise be expected.

7. Conclusions

We conclude that in the samples we have prepared, the nickel atoms do not enter the a-Si host network either substitutionally or interstitially, but that the resulting system contains two distinct amorphous regions; one being a modified semiconducting network, while the other contains both silicon and nickel atoms and is thought to be of higher conductivity. Evidence for two phases in similar systems has also recently been published [20].

These results indicate that the assumption that the MITs observed in a-Si : M systems (where M = transition metal) are of Anderson type, is not

as well founded as previously thought. Indeed, the evidence for cluster formation suggests that the application of classical percolation theory, where conduction occurs via the percolation of electrons along interconnecting regions of enhanced conductivity, may be more appropriate.

We have shown that a knowledge of the structure of a semiconductor : metal system is a necessary prerequisite for a successful description of the conduction mechanism to be made. Measurements on other, related systems are currently in progress.

The authors would like to thank members of the Physics Departments at the Universites of Kent and Leicester, especially S.C. Bayliss, H.S. Derbyshire and N. Piggins, together with G. McTurk for electron microprobe analysis. We also wish to thank the staff at the Daresbury Laboratory, especially W. Myring, for their help. This work was carried out with the aid of a grant from SERC, and A.M. Edwards acknowledges the receipt of a studentship from the University of Kent at Canterbury.

References

[1] K. Morigaki, Phil. Mag. B42 (1980) 979.
[2] M.M. Collver, Sol. St. Commun. 23 (1977) 333.
[3] N.A. Rogachev, V. Smid, J.J. Mares and J. Kristofik, J. Non-Cryst. Sol. 97&98 (1987) 955.
[4] J. Vossen and W.Kern, eds., Thin film processes (Academic Press, London, 1978).
[5] J.D. Joannopoulos and G. Lucovsky, eds., The Physics of Hydrogenated Amorphous Silicon I (Springer, Berlin, 1984).
[6] R.A. Asal, S.C. Bayliss and E.A. Davis, private communication.
[7] E.A. Davis, S.C. Bayliss and R. Asal, to be published.
[8] Synchrotron Radiation, Appendix to the Daresbury Annual Report (1987/88).
[9] W.T. Elam, J.P. Kirkland, R.A. Neiser and P.D. Wolf, Phys. Rev. B38 (1988) 26.
[10] C.D. Garner and S.S. Hasnain, eds., EXAFS for Inorganic Systems (Daresbury Lab. Report DL/SCI/R17, 1981).
[11] C. Morrel, J.T.M. Baines, J.C. Campbell, G.P. Diakun, B.R. Dobson, G.N. Greaves and S.S. Hasnain, eds., Daresbury EXAFS users' manual (1989).
[12] P.A. Lee and J.B. Pendry, Phys. Rev. B11 (1975) 2795.
[13] N. Binsted, S.J. Gurman and J.W. Campbell, SERC Daresbury Laboratory EXCURV88 Program (1988).
[14] S.J. Gurman, N. Binsted and I. Ross, J. Phys. C17 (1984) 143.
[15] R.W. Joyner, K.J. Martin and P. Meehan, J. Phys. C20 (1987) 4005.
[16] B.K. Teo and P.A. Lee, J. Amer. Chem. Soc. 101 (1979) 2815.
[17] R.W.G. Wyckoff, Crystal Structures, Vol. I (Wiley–Interscience, New York, 1963).
[18] J.G. Clabes, Surface Sci. 145 (1984) 87.
[19] R.T. Tung, J.M. Gibson and J.M. Poate, Phys. Rev. Lett. 50 (1983) 429.
[20] J.B. Kortright and A. Bienenstock, Phys. Rev. B37 (1988) 2979.